Construction and Building Materials 147 (2017) 466–477

Contents lists available at ScienceDirect

Construction and Building Materials

journal homepage: www.elsevier.com/locate/conbuildmat

Early-age temperature evolutions in concrete pavements containing microencapsulated phase change materials

Benjamin A. Young [a], Gabriel Falzone [b], Zhenyu She [a], Alexander M. Thiele [a], Zhenhua Wei [b], Narayanan Neithalath [c], Gaurav Sant [b,d,e,*], Laurent Pilon [a,*]

[a] Department of Mechanical and Aerospace Engineering, Henry Samueli School of Engineering and Applied Science, University of California, Los Angeles, CA 90095, United States
[b] Laboratory for the Chemistry of Construction Materials (LC^2), Department of Civil and Environmental Engineering, Henry Samueli School of Engineering and Applied Science, University of California, Los Angeles, CA 90095, United States
[c] School of Sustainable Engineering and the Built-Environment, Arizona State University, Tempe, AZ 85281, United States
[d] Department of Materials Science and Engineering, Henry Samueli School of Engineering and Applied Science, University of California, Los Angeles, CA 90095, United States
[e] California Nanosystems Institute, University of California, Los Angeles, CA 90095, United States

HIGHLIGHTS

- Temperature evolution within early-age pavements containing PCMs was simulated.
- Simulations were supported by experimental calorimetry data.
- Including PCM in the pavement reduces the hydration-induced temperature rise.
- PCMs with larger thermal conductivities are more attractive due to their ability to reduce temperature gradients.
- A design rule for selecting a PCM's melting temperature was proposed.

ARTICLE INFO

Article history:
Received 6 January 2017
Received in revised form 1 April 2017
Accepted 15 April 2017

Keywords:
Phase change materials
Early-age concrete
Cementitious composites
Crack-resistant pavements
Thermal modeling

ABSTRACT

This study examined the benefits of adding microencapsulated phase change materials (PCMs) to concrete pavement sections so as to limit temperature rise and the development of temperature gradients due to exothermic cement hydration reactions and environmental exposure at early-ages. Isothermal calorimetry measurements of the heat generation rate associated with cement hydration as a function of time and temperature were carried out. A transient 1D thermal model of a pavement section was developed to simulate the temporal evolution of temperature within PCM-containing pavement sections exposed to realistic climate conditions. The results highlight that while the low thermal conductivity of typical organic PCMs may be undesirable, the PCM's latent heat capacity ensures substantial reductions in early-age temperature rise and the spatial temperature gradients developed within the pavement. In addition, a selection criterion is proposed to choose a PCM's phase change temperature based on its melting temperature window and the concrete temperature at the time of placement. It is noted that choosing a PCM with a phase change temperature equal to the concrete's placement temperature plus one-half of the melting temperature window provides the largest reduction in peak pavement temperature. The results provide original insights that are needed to design crack-resistant pavements containing PCMs.

1. Introduction

The exothermic nature of cement hydration and exposure to environmental heat results in semi-adiabatic temperature rise and the development of temperature gradients in concrete pavements. Such temperature rise and the subsequent cooling that occurs over the following days can result in thermal cracking in restrained concrete pavements [1,2]. The development of spatial temperature gradients within the pavement (e.g., due to a cooler bottom surface than top surface; coupled with internal heat generation) can result in the development of non-linear (thermal) strain gradients, and the consequent development of tensile stresses, which can ultimately lead to cracking [2]. This is significant, as

* Corresponding authors at: Laboratory for the Chemistry of Construction Materials (LC^2), Department of Civil and Environmental Engineering, Henry Samueli School of Engineering and Applied Science, University of California, Los Angeles, CA 90095, United States (G. Sant).
E-mail addresses: gsant@ucla.edu (G. Sant), pilon@seas.ucla.edu (L. Pilon).

http://dx.doi.org/10.1016/j.conbuildmat.2017.04.150
0950-0618/

Nomenclature

B	hydration rate parameter, unitless
C_c	cement content, kg/m^3
c_p	specific heat, J/kg K
E_a	activation energy, J/mol
ΔH	heat of hydration, J/kg
h	convective heat transfer coefficient, W/m^2 K
h_{sf}	latent heat of fusion, J/kg
k	thermal conductivity, W/m K
L	pavement thickness, m
L_s	soil section thickness, m
Nu	Nusselt number, unitless
q''	heat flux, W/m^2
q''_s	incident solar radiation flux, W/m^2
$\dot{q}$	heat generation rate, W/m^3
R	universal gas constant, J/mol K
Re	Reynolds number, unitless
t	time, s or h
t_{eq}	equivalent age, s or h
$T_p(x,t)$	pavement temperature, °C
$T_{sl}(x,t)$	soil temperature, °C
$T_{sa}(t)$	sol-air temperature, °C
$T_\infty(t)$	outdoor air temperature, °C
T_{pc}	phase change temperature of the PCM, °C
x	distance from pavement surface, m
w/c	water-to-cement ratio, mass basis

Greek symbols

α_s	total hemispherical solar absorptivity
ΔT_{pc}	PCM melting temperature window, °C
ε	total hemispherical emissivity
ϕ_i	volume fraction of material i in composite
ρ	density, kg/m^3
σ	Stefan-Boltzmann constant, W/m^2 K^4
τ	hydration time constant, s or h
θ	degree of hydration, fraction
θ_∞	ultimate degree of hydration, fraction

Subscripts

a	refers to air
c	refers to core material in composite
$c+s$	refers to core-shell microcapsule
eff	refers to effective properties
l	refers to liquid phase
m	refers to matrix material in composite
s	refers to solid phase or shell material in composite
sl	refers to soil

minimizing the temperature and strain gradients (i.e., by ensuring a more uniform internal temperature through the depth of the pavement) would be an important direction toward reducing the risk of thermal cracking. The risk of such early-age thermal cracking is expectedly the highest over the first 7 days when the concrete pavement experiences the most substantial variations in its internal temperature.

In addition to the established, but passive approaches of ice and liquid-N_2 additions that aim to reduce the concrete's temperature at the time of placement [3–5], phase change materials (PCMs) have recently been proposed as a means to mitigate the risk of thermal cracking of concrete [6,7]. PCMs are *temperature programmable* thermal energy storage devices that can store large amounts of latent heat that is associated with melting and solidification processes [8,9]. Specifically, the latent heat offered by PCMs can be used to capture heat released during cement hydration reactions and/or entering the pavement from the environment; thereby reducing the peak temperature attained within the pavement [7]. Furthermore, as the ambient temperature decreases, PCMs can desorb their stored heat, thereby helping to reduce the severity of temperature gradients developed in concrete pavements. Importantly, both of these actions can be designed to occur at and around specific phase change temperatures; as a result of which, PCM-containing cementitious composites can be designed for optimal performance across a range of material compositions and climate locations.

While a promising approach, the thermal behavior of PCM-containing pavements exposed to realistic climatic conditions has not yet been rigorously examined, or modeled. Therefore, the present study aims to: (i) develop a transient one-dimensional (1D) thermal model of a realistic early-age (concrete) pavement section containing microencapsulated PCMs whose input parameters are informed by isothermal calorimetry measurements of heat release within hydrating PCM-cement paste specimens, and (ii) to determine whether the addition of PCMs can reduce the maximum temperature and the temperature gradients developed within the first few days of casting, thereby reducing the thermal cracking risk. The outcomes provide new insights that are needed to ascertain the optimal PCM characteristics that mitigate the risk of thermal cracking in restrained concrete pavements.

2. Background

2.1. Modeling heat generation in concrete pavements at early-ages

Several studies have developed thermal models to predict transient temperature evolutions in pavement sections exposed to the outdoor environment [10–21]. These models have been developed for both mature concrete sections [10–17] as well as for early-age concrete, for time periods following concrete placement until seven days [18–21], when heat generation resulting from cement hydration reactions is a significant contributor to thermal behavior. Since the subgrade can serve as a heat-sink, such models describe transient temperature evolutions both within the pavement section, and within an underlying soil layer [16].

To assess the effects of cement hydration on early-age temperature evolutions, it is crucial to account for the degree of hydration (i.e., extent of reaction) of the cement [22,23]. In general, this quantity depends on both time and the temperature history at a given location, since the reaction rate increases with temperature [5]. Hansen and Pederson [24] proposed that the effects of both time and temperature can be accounted for via an "equivalent age" $t_{eq}(x,t)$ defined as,

$$t_{eq}(x,t) = \int_0^t \exp\left[-\frac{E_a}{R}\left(\frac{1}{T(x,t)} - \frac{1}{T_{ref}}\right)\right] dt \quad (1)$$

where E_a is the activation energy, $R = 8.314$ J/mol K is the ideal gas constant, and T_{ref} is the reference temperature. The equivalent age concept, based on the Arrhenius formalism of assuming reaction rate has an exponential relationship with temperature, has been widely applied to predict the degree of hydration and strength development in concrete [19–21,25–29]. The degree of hydration $\theta(t_{eq})$ can be approximated as a function of the equivalent age as [21,29],

$$\theta(t_{eq}) = \theta_\infty \exp\left[-\left(\frac{\tau}{t_{eq}}\right)^B\right] \quad (2)$$

where the parameters θ_∞, B, and τ are assessed by fitting Eq. (2) to experimental data of $\theta(t_{eq})$.

2.2. Thermal modeling of PCM-containing cementitious composites

The thermal behavior of composites consisting of spherical inclusions embedded in a continuous matrix (i.e., analogous to the composite "PCM + concrete" pavement section considered herein) was shown to be accurately predicted by simulating an equivalent homogeneous material with appropriate effective thermal properties [30,31]. Based on robust thermodynamic arguments, the effective volumetric heat capacity of the composite was computed as a volume-weighted average of the different heat capacities [31],

$$(\rho c_p)_{eff}(T) = \phi_c(\rho c_p)_c(T) + \phi_s(\rho c_p)_s + (1-\phi_c-\phi_s)(\rho c_p)_m \quad (3)$$

where ϕ_c and ϕ_s are the volume fractions of the core and shell components of the microencapsulated PCM, respectively. The effective thermal conductivity of the composite was computed using Felske's model as [32],

$$k_{eff} = \frac{k_m(1-\phi_c-\phi_s)\left[6+4\frac{\phi_s}{\phi_c}+2\frac{\phi_s k_c}{\phi_c k_s}\right] + (1+2\phi_c+2\phi_s)\left[3+\frac{\phi_s}{\phi_c}k_c+2\frac{\phi_s}{\phi_c}k_s\right]}{(2+\phi_c+\phi_s)\left[3+2\frac{\phi_s}{\phi_c}+\frac{\phi_s k_c}{\phi_c k_s}\right] + (1-\phi_c-\phi_s)\left[\left(3+\frac{\phi_s}{\phi_c}\right)\frac{k_c}{k_m}+2\frac{\phi_s k_s}{\phi_c k_m}\right]}. \quad (4)$$

To accurately capture the effect of phase change on temperature development in PCM-concrete composites, the effective heat capacity method [33] can be used to describe the PCM's specific heat $c_{p,c}(T)$ as a rectangular step function of temperature, i.e.,

$$c_{p,c}(T) = \begin{cases} c_{p,c,s} & \text{for } T < T_{pc} - \Delta T_{pc}/2 \\ c_{p,c,s} + \frac{h_{sf}}{\Delta T_{pc}} & \text{for } T_{pc} - \Delta T_{pc}/2 \leqslant T \leqslant T_{pc} + \Delta T_{pc}/2 \\ c_{p,c,l} & \text{for } T > T_{pc} + \Delta T_{pc}/2 \end{cases} \quad (5)$$

where $c_{p,c,s}$ and $c_{p,c,l}$ are the specific heats (in J/kg K) of the PCM in the solid and liquid states, respectively, h_{sf} is its latent heat of fusion (in J/kg), T_{pc} is the PCM's melting temperature, and ΔT_{pc} is the melting temperature window over which phase change occurs. It should be noted that the use of a step function or Gaussian function to describe phase change behavior results in little, if any difference in terms of simulated thermal behavior [34]. The effective heat capacity method allows one to easily parameterize and examine the influences of different PCM properties including: h_{sf}, T_{pc}, or ΔT_{pc}. This method was previously validated against an exact solution for the 1D Stefan problem of heat conduction in a paraffin slab undergoing phase change [31,34].

3. Materials and methods

3.1. Material synthesis

A microencapsulated phase change material (MPCM24D, Microtek Laboratories Inc.) consisting of a paraffinous core encapsulated within a melamine-formaldehyde (MF) shell was used. The PCM featured a melting temperature around 24 °C. An ASTM C150 [35] compliant Type I/II ordinary portland cement (OPC) was used. The OPC featured a nominal composition of: 57.8% C_3S, 18.2% C_2S, 5.5% C_3A and 9.1% C_4AF as determined by X-ray fluorescence (XRF). The cementitious composites were mixed in accordance with ASTM C305 [36]. First, cement pastes were prepared by mixing OPC with deionized (DI) water at water-to-cement ratios (w/c, mass basis) of 0.45 and 0.55. Microencapsulated PCM was added to the anhydrous OPC and mixed by hand prior to the addition of DI water. The cementitious composites containing PCM were prepared for microencapsulated PCM volume fractions $\phi_{c+s} = 0.05$ and 0.10. The desired microencapsulated PCM volume fraction ϕ_{c+s} was achieved by adding the required mass of microencapsulated PCM to the mixture based on its density $\rho_{c+s} = 900$ kg/m^3 [37].

3.2. Experimental procedures

An isothermal calorimeter (Tam Air, TA Instruments) was used to measure the thermal power (i.e., heat flow in W) and the heat of hydration of cementitious composites for different w/c and PCM volume fractions. The measurements were performed as described in ASTM C1702 [25] for 7 days. The testing temperature of the isothermal calorimeter was set to 15, 30, or 45 °C in order to observe different reaction rates and states of the PCM (i.e., solid or liquid). Reference specimens of DI water were prepared with equivalent thermal mass to the cementitious composites and used to measure the baseline heat flow signal. The baseline signal was subtracted from the measured heat flow of the cementitious composites. All mixture ingredients were conditioned to the relevant test temperature (15, 30, or 45 °C) before mixing. Immediately after mixing, approximately 10 g of each cementitious specimen was loaded into a 20 mL glass ampoule, sealed, and then placed into the calorimeter block.

4. Analysis

4.1. Schematic and assumptions

Fig. 1 illustrates the simulated pavement section of thickness $L = 0.25$ m similar to that of a typical U.S. highway pavement [38] and soil section of thickness $L_s = 2$ m along with the associated coordinate system. The pavement section had effective properties k_{eff} and $(\rho c_p)_{eff}(T_p)$ and experienced a local rate of heat generation per unit volume $\dot{q}(x,t)$. The soil layer had a thermal conductivity k_{sl} and volumetric heat capacity $(\rho c_p)_{sl}$. The upper surface of the pavement ($x = 0$) was exposed to convection with the ambient air at temperature T_∞ with convective heat transfer coefficient h. It was also exposed to solar radiation flux $q''_s(t)$ (in W/m^2), and exchanged thermal radiation with the sky at temperature T_{sky}. The pavement surface had a total hemispherical solar absorptivity α_s and a total hemispherical emissivity ε. The bottom of the soil section ($x = L + L_s$) was assumed to be at a constant temperature T_g.

To make the problem mathematically tractable, it was assumed that: (i) one-dimensional (1D) heat conduction in the x-direction prevailed, (ii) all the material properties were constant and isotropic except for the temperature-dependent specific heat of the PCM, (iii) the PCM's specific heat was the same in the solid and liquid states, i.e., $c_{p,c,s} = c_{p,c,l}$, (iv) the convective heat transfer coefficient h at the pavement surface remained constant, (v) radiation exchange between the pavement and the sky was unobstructed and from a small surface to large surroundings, and, (vi) evaporative cooling at the pavement surface was negligible.

4.2. Governing equations

The temperature in the pavement section $T_p(x,t)$ was governed by the 1D transient heat diffusion equation with heat generation [39],

$$(\rho c_p)_{eff}(T_p)\frac{\partial T_p}{\partial t} = k_{eff}\frac{\partial^2 T_p}{\partial x^2} + \dot{q}(x,t) \quad (6)$$

where $\dot{q}(x,t)$ is the local rate of heat generation per unit volume (in W/m^3). Similarly, the soil temperature $T_{sl}(x,t)$ was also governed by

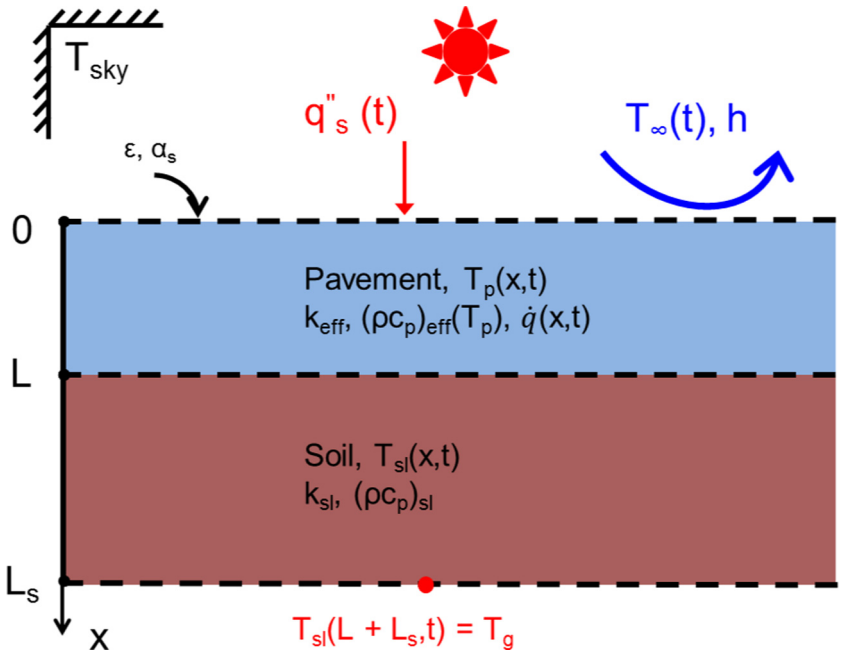

Fig. 1. A schematic of simulated pavement and soil sections of thickness $L = 0.25$ m, corresponding to a typical highway pavement in the U.S. [38], and $L_s = 2$ m, respectively. The upper surface of the pavement ($x = 0$) was exposed to convective heat transfer and thermal radiation exchanges with the outdoor environment, while the bottom of the soil section ($x = L + L_s$) was held at a constant temperature T_g.

the transient heat diffusion equation but without heat generation, i.e.,

$$(\rho c_p)_{sl}\frac{\partial T_{sl}}{\partial t} = k_{sl}\frac{\partial^2 T_{sl}}{\partial x^2}. \tag{7}$$

Additionally, the pavement equivalent age $t_{eq}(x,t)$ can be expressed in differential form as,

$$\frac{\partial t_{eq}}{\partial t} = \exp\left[-\frac{E_a}{R}\left(\frac{1}{T_p(x,t)} - \frac{1}{T_{ref}}\right)\right]. \tag{8}$$

4.3. Initial and boundary conditions

At time $t = 0$, the temperature in the pavement section was taken to be uniform and equal to an initial temperature T_{init}, i.e.,

$$T_p(x,0) = T_{init}. \tag{9}$$

Additionally, the soil section was assumed to have a uniform initial temperature equal to the ground temperature T_g,

$$T_{sl}(x,0) = T_g. \tag{10}$$

To account for the fact that some hydration had taken place before the concrete was placed, the pavement was assumed to be at an initial equivalent age $t_{eq}(x,0) = 0.5$ h though in practice, due to the time elapsed during transportation, this number may be slightly higher. A heat flux boundary condition was imposed at the upper pavement surface ($x = 0$) to include the effects of convective heat transfer, absorption of incident solar radiation, and thermal emission. Both convection and incident solar radiation can be accounted for by introducing the sol-air temperature $T_{sa}(t)$ as [40],

$$T_{sa}(t) = T_\infty(t) + \frac{\alpha_s q_s''(t)}{h} \tag{11}$$

where α_s is the pavement's total hemispherical solar absorptivity, $q_s''(t)$ is the incident solar radiation flux, and h is the convective heat transfer coefficient between the pavement surface and the outdoor air at T_∞. Then, the heat flux at $x = 0$ can be expressed as,

$$-k_{eff}\frac{\partial T_p}{\partial x} = h[T_{sa}(t) - T_p(0,t)] - \varepsilon\sigma[T_p(0,t)^4 - T_{sky}^4] \tag{12}$$

where ε is the total hemispherical emissivity of the pavement surface, $\sigma = 5.67 \times 10^{-8}$ W/m$^2 \cdot$ K^4 is the Stefan-Boltzmann constant, and T_{sky} is the average sky temperature, taken as 2 °C [39]. The bottom surface of the soil section ($x = L + L_s$) remained at T_g, i.e.,

$$T_{sl}(L + L_s, t) = T_g. \tag{13}$$

Finally, the temperature and heat flux were continuous across the pavement-soil interface such that

$$T_p(L,t) = T_{sl}(L,t) \quad \text{and} \quad k_{eff}\frac{\partial T_p}{\partial x}(L,t) = k_{sl}\frac{\partial T_{sl}}{\partial x}(L,t). \tag{14}$$

4.4. Heat generation rate

The total heat released per unit volume of the concrete from exothermic cement-water reactions at a given location can be written in terms of the degree of hydration $\theta(t_{eq})$ and equivalent age $t_{eq}(x,t)$ as [21],

$$Q(t_{eq}) = C_c \Delta H \theta(t_{eq}) \tag{15}$$

where ΔH is enthalpy of reaction (in J/kg) and C_c is the cement content, i.e., the mass of cement per unit volume of the concrete (in kg/m^3). The enthalpy of reaction of cement can be calculated as the mass-averaged enthalpy of reaction (with water) of each mineralogical phase,

$$\Delta H = m_{C_3S}\Delta H_{C_3S} + m_{C_2S}\Delta H_{C_2S} + m_{C_3A}\Delta H_{C_3A} + m_{C_4AF}\Delta H_{C_4AF} \tag{16}$$

where m_i and ΔH_i are the mass fraction and enthalpy of reaction, respectively, of each constituent in cement, namely C_3S, C_2S, C_3A, and C_4AF [41,42]. The mass fraction of each constituent was obtained by X-ray fluorescence measurements. The resulting ΔH was calculated as 475 kJ/kg for the cement used in this study. Then, by combining Eqs. (1) and (2) along with Eq. (15) the instantaneous rate of heat generation $\dot{q}(x,t)$ (in W/m^3) can be expressed as [21],

$$\dot{q}(x,t) = \frac{C_c \Delta H \theta_\infty B}{t_{eq}(x,t)} \left(\frac{\tau}{t_{eq}(x,t)}\right)^B \times \exp\left[-\left(\frac{\tau}{t_{eq}(x,t)}\right)^B\right] \exp\left[-\frac{E_a}{R}\left(\frac{1}{T_p(x,t)} - \frac{1}{T_{ref}}\right)\right]. \quad (17)$$

4.5. Constitutive relationships

Table 1 summarizes the thermal conductivity k, density ρ, and specific heat c_p of concrete, melamine-formaldehyde shell (MF), PCM core, and soil used in the simulations. The PCM's latent heat of fusion was taken as $h_{sf} = 180$ kJ/kg [43]. The effective volumetric heat capacity of the pavement section was calculated using a volume average as in Eq. (3), while the effective thermal conductivity was determined using Eq. (4) [32]. The effective heat capacity method outlined by Eq. (5) was used to determine the PCM's specific heat $c_{p,c}(T)$ as a function of its temperature. The cement content C_c was taken as 586 kg/m^3 corresponding to laboratory formulated mortars with a total inclusion (fine aggregate) volume fraction of 55%. Note that in a typical concrete, the inclusion volume fraction can be as high as 75% [3], which would result in a lower cement content.

Convective heat transfer at the upper pavement surface was modeled as laminar forced convection over a flat plate using the correlation for the surfaced-averaged Nusselt number [39],

$$\overline{Nu}_L = \frac{hL_c}{k} = 0.664 Re_L^{1/2} Pr^{1/3} \quad (18)$$

where $Re_L = u_\infty L_c / v$ is the Reynolds number based on the wind velocity u_∞ and Pr is the fluid Prandtl number. The thermal conductivity k_a, kinematic viscosity v_a, and Prandtl number Pr_a of air at 27 °C were taken as 0.03 W/m K, 1.58×10^{-5} m^2/s, and 0.707 respectively [39]. Here, the characteristic length L_c was taken as 1.5 m to represent the area-to-perimeter ratio [14] for a pavement section of "infinite" length and typical width of 3 m [44], while the average wind speed u_∞ was taken as 2.5 m/s [45]. The resulting convective heat transfer coefficient h obtained from Eq. (18) was 5 W/m^2 K. Note that this value is close to that of 3.6 W/m^2 K predicted by the correlation suggested by Wolfe et al. [46] based on experimental measurements of the convective heat transfer coefficient at a pavement surface.

The sol-air temperature $T_{sa}(t)$ imposed in Eq. (12) was obtained from Climate Consultant for California Climate Zone 9 (Los Angeles, CA) [45]. Fig. 2 plots the outdoor air temperature $T_\infty(t)$ and the sol-air temperature $T_{sa}(t)$ corresponding to: (a) September 24th and (b) March 2nd in Los Angeles, CA. These days were selected because they were the hottest and coldest days, respectively, based on historically averaged weather data. The ground temperature T_g was imposed as 19 °C [45]. The initial temperature of the pavement section was $T_{init} = 40$ °C. Finally, the total hemispherical solar absorptivity of the pavement α_s was taken as 0.6, while its total hemispherical emissivity was 0.9, as reported in the literature for plain concrete [39].

4.6. Method of solution

The transient 1D governing Eqs. (6)–(8) were solved along with the corresponding boundary and initial conditions using a semi-implicit finite difference method [39]. The solution was considered to be numerically converged when the resulting pavement temperature (i.e., at any time or spatial location) differed by no more than 1% after reducing the nodal spacing Δx or the time step Δt by a factor of 2. A nodal spacing $\Delta x = 5.8$ mm and time step $\Delta t = 300$ s were sufficient to provide a converged solution.

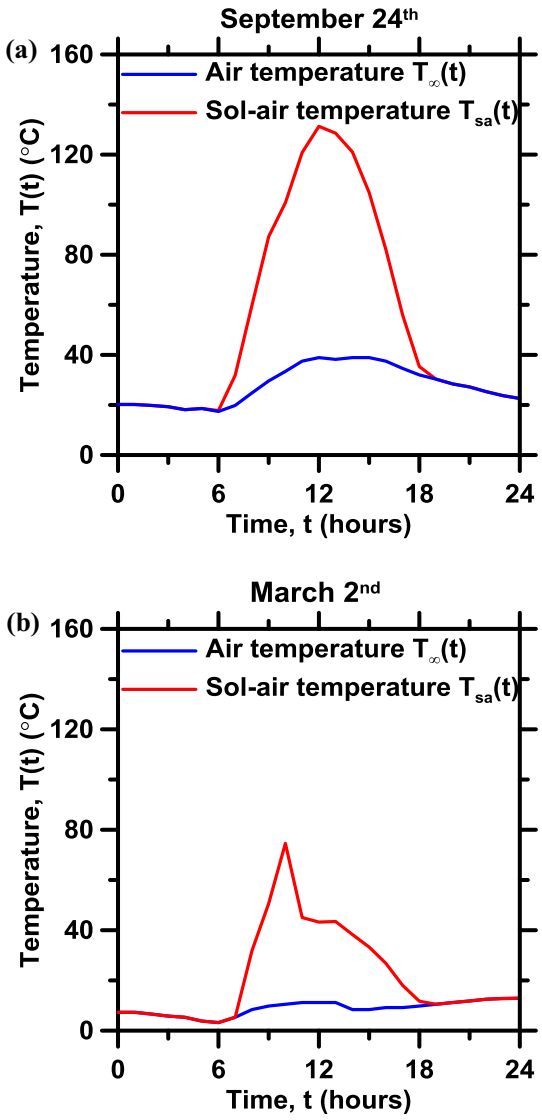

Fig. 2. The outdoor air temperature $T_\infty(t)$ and sol-air temperature $T_{sa}(t)$ corresponding to (a) September 24th and (b) March 2nd in Los Angeles, CA.

4.7. Data processing

Two criteria were defined to evaluate the thermal performance of the pavement section. First, the maximum pavement temperature $T_{max}(t)$ was defined for each instant as,

Table 1
Thermal conductivity k, density ρ, and specific heat c_p of concrete, melamine-formaldehyde (MF), PCM, and soil.

Material	Subscript	k (W/m K)	ρ (kg/m^3)	c_p (J/kg K)	Ref.
Concrete	m	1.4	2330	880	[39]
MF-shell	s	0.49	930	2250	[56]
PCM-core	c	0.21	860	2590	[43,57]
Soil	sl	0.52	2050	1840	[39]

$$T_{\max}(t) = \max_{\forall x}[T_p(x,t)]. \quad (19)$$

Second, the maximum temperature gradient $T_{x,\max}(t)$ was defined for each instant as,

$$T_{x,\max}(t) = \max_{\forall x}\left[\frac{\partial T_p}{\partial x}(x,t)\right]. \quad (20)$$

Finally, the overall maximum (peak) temperature and temperature gradient attained within the pavement section during the 24-h simulation period were also recorded and defined as,

$$T_{peak} = \max_{\forall t}[T_{\max}(t)] \quad \text{and} \quad T_{x,peak} = \max_{\forall t}[T_{x,\max}(t)]. \quad (21)$$

5. Results and discussion

5.1. Isothermal calorimetry

Fig. 3a displays heat flow as a function of time from the time of initial mixing of cement and water measured at different temperatures, namely 15, 30, and 45 °C, and with PCM volume fraction ϕ_{c+s} equal to 0 or 10%. Expectedly, increasing the temperature accelerated cement hydration, manifesting as a shortened induction period and elevated maximum heat flow. The addition of PCMs was observed to have no influence on the kinetics of reactions [7]. This indicates that the PCM microcapsules induced no acceleratory filler effect on cement hydration; either on account of their small specific surface area or on account of featuring surface properties unfavorable for C-S-H nucleation [47]. To further evaluate the effects of PCM on the degree of hydration, Fig. 3b plots the time-dependent degree of hydration $\theta(t)$ for cementitious specimens with w/c = 0.45 or 0.55 and PCM volume fraction ϕ_{c+s} of 0, 5, or 10%. At a fixed temperature (i.e., T = 30 °C), $\theta(t)$ did not show significant dependence on either w/c or ϕ_{c+s}. It should be noted that the lack of dependence on w/c is expected when sufficient space for the formation of hydration products, and water are available, i.e., for w/c > 0.42 [42].

The activation energy of cement hydration was calculated using an Arrhenius approach via the equivalent age concept expressed in Eq. (1) and assuming a uniform temperature in the sample. The activation energy E_a was estimated from the slope of the degree of hydration θ versus 1000/T plot, for reaction times corresponding to 6, 12, 18, 24 h at 30 °C. Particular attention was paid to the first 24 equivalent hours of hydration when reactions are most sensitive

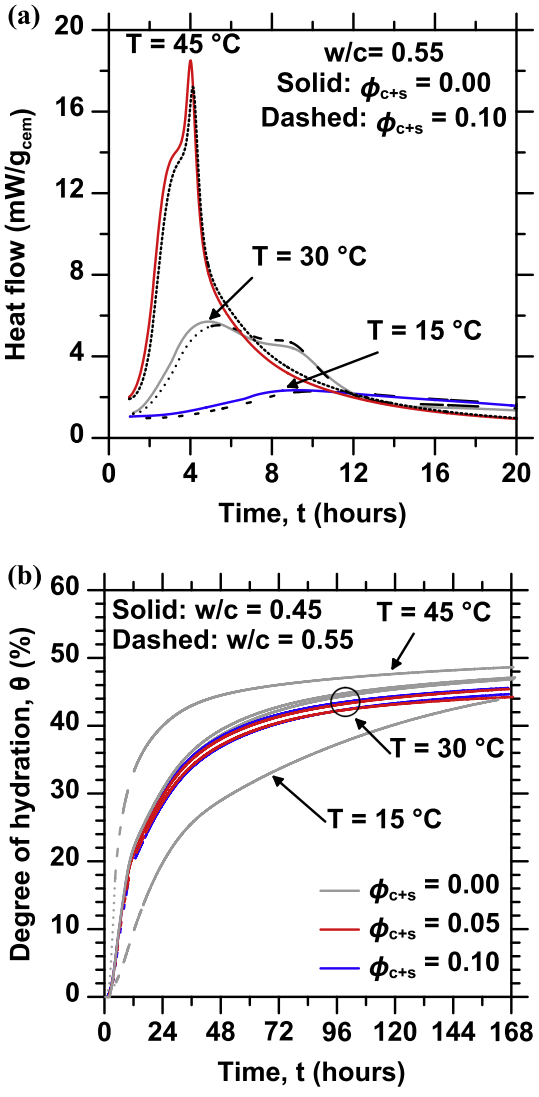

Fig. 3. Representative heat flow profiles for cement pastes (w/c = 0.55) with and without PCM cured at different temperatures, and, (b) the degree of hydration (reaction) of the cementitious specimens as a function of time.

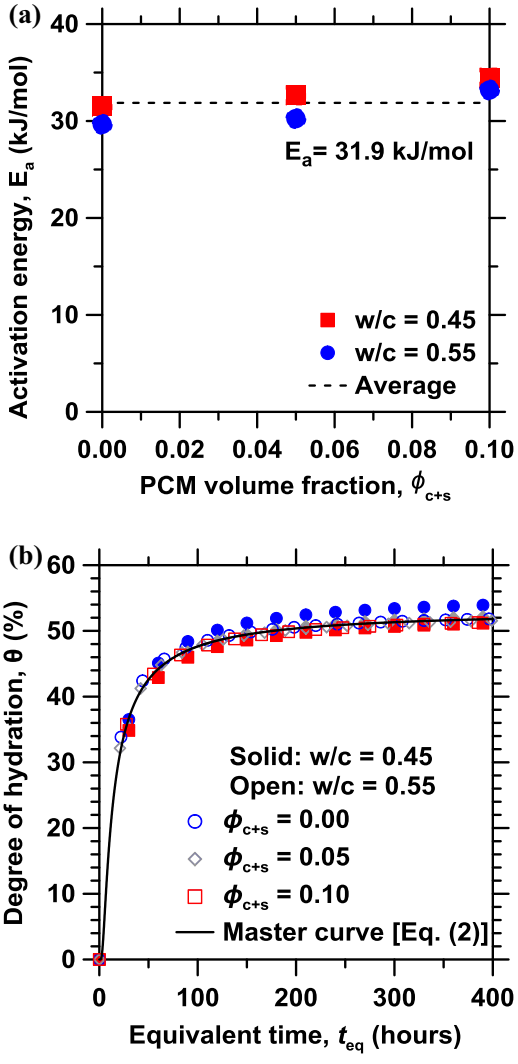

Fig. 4. (a) The activation energy of cement hydration as a function of PCM volume fraction, and, (b) the degree of cement hydration $\theta(t_{eq})$ as a function of equivalent age t_{eq}. The master curve applies to all mixtures regardless of PCM dosage and w/c.

to the effects of temperature. For example, Fig. 4a shows the activation energy as a function of PCM dosage for mixtures at both $w/c = 0.45$ and 0.55. It indicates that the activation energy had little dependence on ϕ_{c+s}. The average activation energy for cement hydration was therefore taken as 31.9 kJ/mol.

Fig. 4 displays the measured degree of hydration $\theta(t_{eq})$ as a function of equivalent age t_{eq} for varying w/c and ϕ_{c+s} for a reference temperature $T_{ref} = 30\,^{\circ}C$ (chosen arbitrarily). Also shown is the resulting degree of hydration "master curve" obtained by fitting Eq. (2) to all experimental data. The curve fit parameters that produced the best fit were $\theta_{\infty} = 0.495$, $B = 0.9$, and $\tau = 11.4$ h. The small variation of experimental measurements from the master curve indicates that the PCM microcapsules do not influence degree of hydration, and broadly function as inert inclusions. Overall, these results indicate that the master curve can be used to describe $\theta(t_{eq})$ for any PCM volume fraction ϕ_{c+s} between 0 and 10% and w/c between 0.45 and 0.55, so long as the activation energy is known. Thus, the values of $\theta_{\infty} = 0.495$, $B = 0.9$, and $\tau = 11.4$ h as determined from fitting the experimentally measured isothermal calorimetry data were used in Eq. (17) to determine the instantaneous rate of heat generation in the numerical model.

5.2. Pavement temperature evolutions

Fig. 5 plots the predicted maximum temperature $T_{max}(t)$ and maximum local temperature gradient $T_{x,max}(t)$ developed within a pavement section exposed to the sol-air temperature corresponding to September 24th in Los Angeles, CA, for a placement

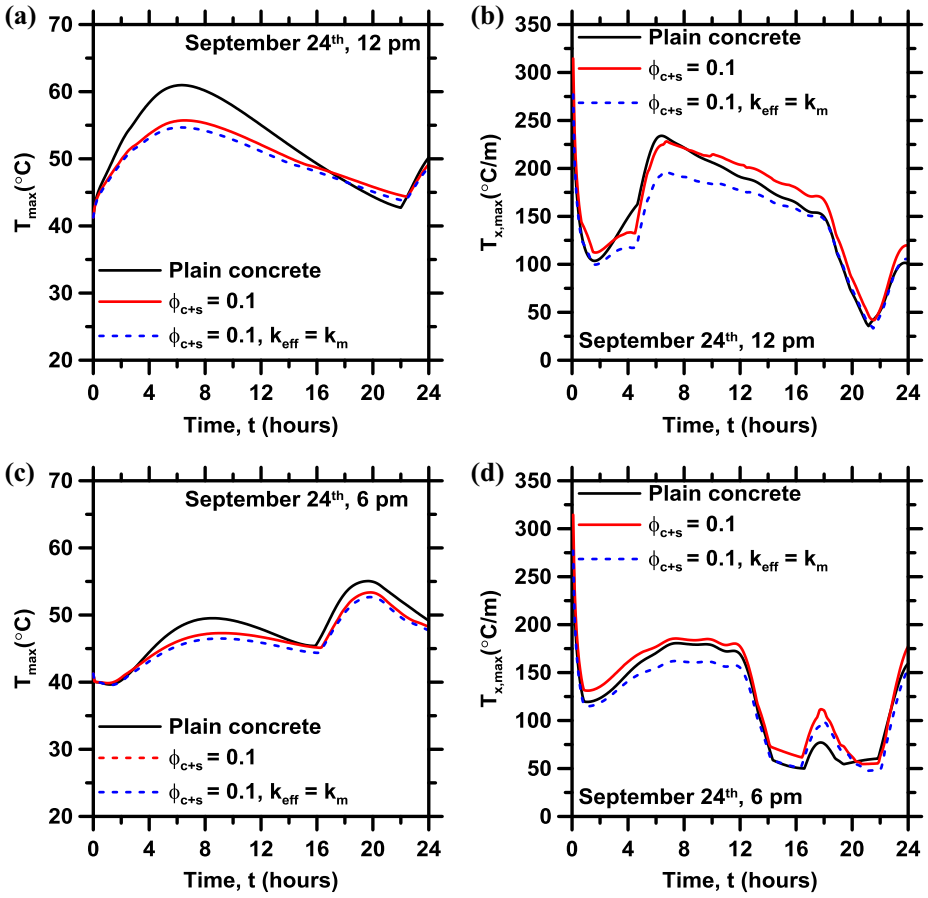

Fig. 5. The maximum temperature $T_{max}(t)$ and local temperature gradient $T_{x,max}(t)$ developed within pavement sections exposed to outdoor temperature and solar irradiation corresponding to September 24th in Los Angeles, CA placed at either (a–b) 12 pm or (c–d) 6 pm. The results shown are for a plain concrete pavement section and sections with 10 vol.% microencapsulated PCM. The PCM's melting temperature T_{pc} was 45 °C and the melting temperature window ΔT_{pc} was 8 °C. The initial pavement temperature was taken as $T_{init} = 40\,^{\circ}C$.

Table 2
The peak temperature T_{peak} and temperature gradient $T_{x,peak}$ developed within the first 24 h after placement for plain concrete or PCM-composite pavement sections exposed to outdoor temperature and solar irradiation corresponding to September 24th or March 2nd in Los Angeles, CA.

Day	Placement time	T_{peak} (°C)		$T_{x,peak}$ (°C/m)	
		Plain concrete	$\phi_{c+s} = 0.1$	Plain concrete	$\phi_{c+s} = 0.1$
September 24th	12 am	60	57	190	174
	6 am	66	61	230	198
	12 pm	61	55	234	197
	6 pm	55	53	181	162
March 2nd	12 am	47	45	196	185
	6 am	52	48	203	185
	12 pm	50	47	205	186
	6 pm	47	45	194	180

time of either 12 pm (a–b) or 6 pm (c–d) for: (i) a plain concrete pavement or (ii) a pavement with 10 vol.% microencapsulated PCM. The PCM melting temperature T_{pc} was fixed at 45 °C, and the melting temperature window ΔT_{pc} was fixed at 8 °C, i.e., PCM melting/freezing took place between 41 °C and 49 °C. The choice of PCM melting temperature was made such that the entire phase change temperature window fell between the initial pavement temperature $T_{init} = 40$ °C and the maximum temperature attained by the plain concrete section, which was around 55–60 °C. Fig. 5a shows that for a placement time of 12 pm, a single large peak in the pavement temperature was observed around 6 h after placement. This can be attributed to the peak of heat generation from hydration occurring near the same time as the peak outdoor temperature and solar irradiation. By contrast, for a placement time of 6 pm (Fig. 5c), there were two separate peaks in $T_{\max}(t)$ corresponding to (i) the peak of heat generation, and (ii) the peak outdoor temperature and solar irradiation of the following day - wherein the subsequent peak was in fact more substantial than the hydration heat peak. In each case, both the maximum temperature and maximum local temperature gradient reached their peak values within the first 24 h of placement.

Fig. 5 indicates that for both placement times considered, the peak temperature was around 5 °C lower for the PCM-containing pavement section as compared to the plain concrete section. However, the addition of 10 vol.% PCM adversely affected the maximum temperature gradient (Fig. 5b and d), compared with the plain concrete section. This is because the PCM microcapsules, on account of their low thermal conductivity, acted as thermal insulators, thereby preventing the dissipation of heat through the pavement surface and the subgrade. Indeed, the inclusion of 10 vol.% PCM with thermal conductivity $k_c = 0.21$ W/m K reduced the thermal conductivity of the pavement section from $k_m = 1.4$ W/m K to $k_{eff} = 1.2$ W/m K, i.e., a reduction of around 15%.

To distinguish the effects of the PCM's latent heat capacity from that of the reduced thermal conductivity, Fig. 5 also shows the maximum temperature $T_{\max}(t)$ and temperature gradient $T_{x,\max}(t)$ obtained from simulating a pavement section with 10 vol.% PCM, but with an effective thermal conductivity equal to that of the plain concrete k_m. In this case, the maximum temperature gradient was reduced by up to 16% or 11% compared with that of the plain concrete section for placement times of 12 pm and 6 pm, respectively. To continue examining the benefits of PCM latent heat and given the limited effect of the thermal conductivity difference on the maximum temperature within the section (see Fig. 5a), the PCM-composite pavement section was treated as having an effective thermal conductivity k_{eff} equal to the plain concrete value of $k_m = 1.4$ W/m K for the remainder of this study. In practice, this could be achieved by: (i) selecting a PCM with a larger thermal conductivity, (ii) selecting a PCM encapsulated within a higher thermal conductivity shell structure [48,49], (iii) impregnating PCM directly into porous aggregates [50], and/or, (iv) adding inclusions with large(r) thermal conductivity, such as quartz sand or graphite, to compensate for the loss in thermal conductivity caused by the addition of PCM microcapsules. These results also

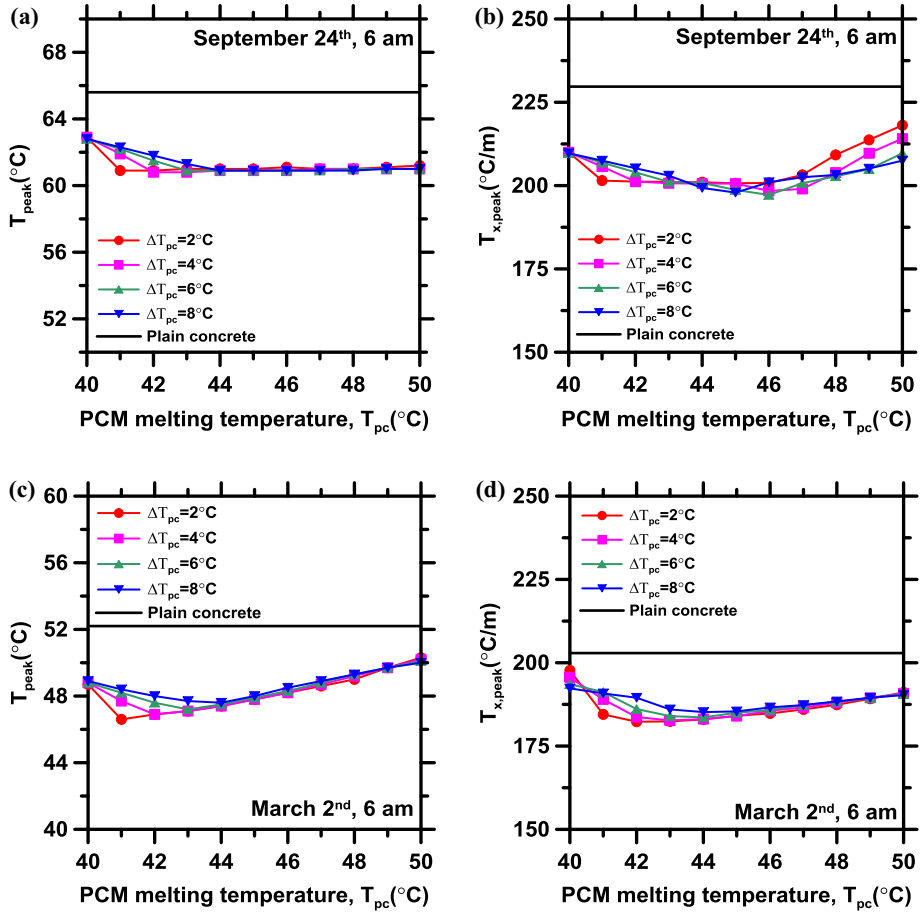

Fig. 6. The effect of PCM melting temperature T_{pc} and melting temperature window ΔT_{pc} on the peak temperature T_{peak} and the local temperature gradient $T_{x,peak}$ attained within a composite pavement section placed at 6 am on (a–b) September 24th or (c–d) March 2nd. The PCM volume fraction was $\phi_{c+s} = 0.1$ and its latent heat of fusion was $h_{sf} = 180$ kJ/kg.

suggest that inorganic PCMs, which tend to have larger thermal conductivities than organic PCMs [51] - only if chemical passivity can be ensured – may be better suited for use in pavement sections.

Table 2 shows the peak temperature T_{peak} and temperature gradient $T_{x,peak}$ attained within the first 24 h of placement for plain concrete or PCM-composite pavement sections exposed to outdoor weather conditions corresponding to either September 24th or March 2nd in Los Angeles, CA. Four different placement times (12 am, 6 am, 12 pm, and 6 pm) were investigated. Table 2 indicates that the inclusion of 10 vol.% PCM reduced the peak temperature T_{peak} in all cases. In particular, the inclusion of PCM reduced the peak temperature the most on September 24th for placement times of 6 am and 12 pm. The peak temperature gradient attained within the pavement was also lower for the PCM-composite pavement section in all cases considered. Here again, the addition of PCM was most beneficial in the September 24th case for placement times of 6 am and 12 pm, reducing the peak temperature gradient by 14% and 16%, respectively. Overall, these results establish that including PCM in pavement sections poured in climates such as that of Los Angeles, CA can provide a noticeable benefit in reducing the peak temperature and temperature gradient developed within the pavement at early-ages; so long as the effective thermal conductivity of the pavement is not substantially reduced.

5.3. Parametric study

The following section presents a parametric study aimed at elucidating the effects of various material and mixture parameters on the thermal performance of a PCM-composite pavement section, namely (i) PCM melting temperature T_{pc} and melting temperature window ΔT_{pc}, (ii) PCM volume fraction ϕ_{c+s}, (iii) PCM latent heat of fusion h_{sf}, and (iv) the initial placement temperature of the concrete T_{init}. Here, the effective thermal conductivity k_{eff} of the composite pavement section was again assumed to be equal to 1.4 W/m K corresponding to that of a plain concrete section.

5.3.1. Effect of PCM melting temperature and melting temperature window

Fig. 6 plots the peak pavement temperature T_{peak} and peak temperature gradient $T_{x,peak}$ within a PCM-composite pavement section for PCM volume fraction $\phi_{c+s} = 0.1$ as a function of the PCM's melting temperature T_{pc} ranging from 40 °C to 50 °C. The outdoor weather conditions corresponded either to (a–b) September 24th or (c–d) March 2nd in Los Angeles, CA. The placement time was 6 am in both cases. Different values of PCM melting temperature window ΔT_{pc} ranging from 2 °C to 8 °C were also considered. For reference, the peak temperature and peak temperature gradient attained within a plain concrete pavement section exposed to the same climate conditions are also shown. Fig. 6 shows that T_{peak} and $T_{x,peak}$ did not show a significant dependence on the width of the melting temperature window ΔT_{pc}, provided that the window is fully encompassed. Fig. 6a and c also show that for both cases considered, the peak temperature was reduced the most when the lower bound of the PCM phase change window was near the pavement's initial temperature $T_{init} = 40$ °C. In other words, the optimal PCM melting temperature was,

$$T_{pc,opt} = T_{init} + \frac{\Delta T_{pc}}{2}. \quad (22)$$

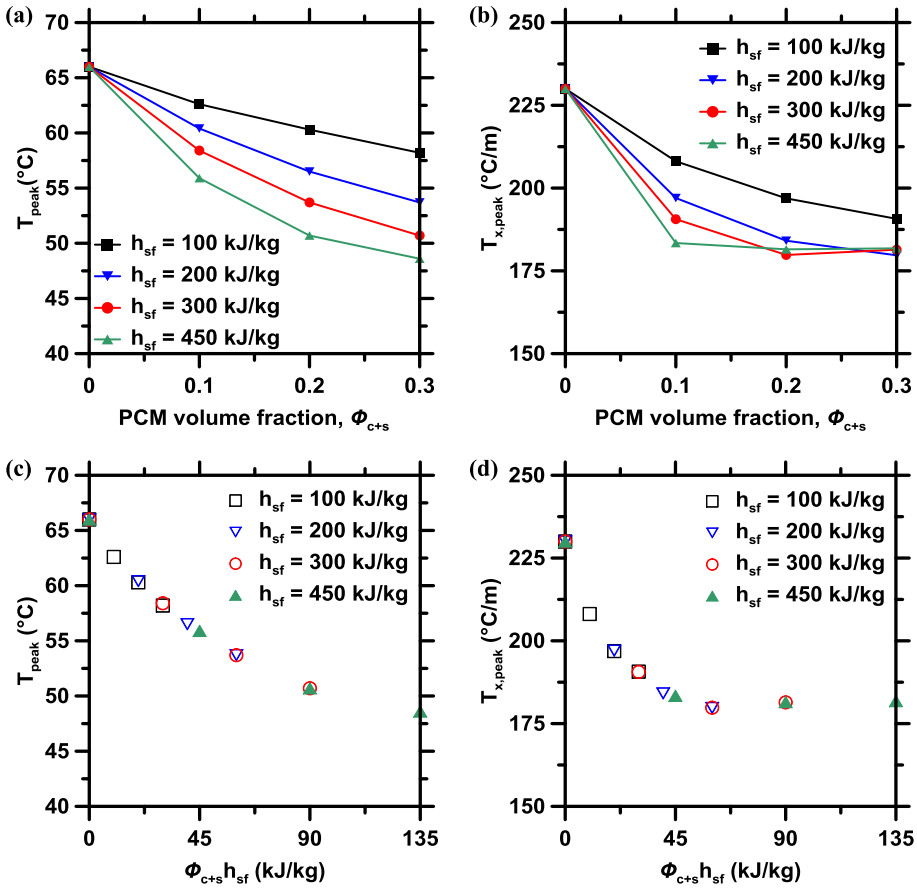

Fig. 7. The effect of (a–b) microencapsulated PCM volume fraction ϕ_{c+s} and PCM latent heat of fusion h_{sf} as well as (c–d) the product $\phi_{c+s}h_{sf}$ on the peak temperature and temperature gradient attained within a composite pavement section placed on September 24th at 6 am. Here, the PCM's melting temperature was $T_{pc} = 45$ °C and the melting temperature window was $\Delta T_{pc} = 8$ °C.

Fig. 6b and d indicate that selection of the PCM melting temperature near this optimum also provides the largest possible reduction in peak temperature gradient.

5.3.2. Effect of PCM volume fraction and latent heat of fusion

Fig. 7 plots (a) the peak temperature T_{peak} and (b) the peak temperature gradient $T_{x,peak}$ attained within a PCM-composite pavement section as a function of the PCM volume fraction ϕ_{c+s} and its latent heat of fusion h_{sf}. Fig. 7a establishes that the peak temperature decreased with increasing PCM volume fraction, and decreased more sharply with increasing PCM latent heat. Fig. 7b shows that the peak temperature gradient also decreased with increasing PCM volume fraction when h_{sf} was between 100 and 200 kJ/kg. However, for $h_{sf} = 300$ or 450 kJ/kg, $T_{x,peak}$ was no longer reduced by further increases in the PCM dosage once ϕ_{c+s} reached 0.2, suggesting that there is a limit to which the temperature gradient can be reduced by latent heat storage alone.

Fig. 7 also plots (c) T_{peak} and (d) $T_{x,peak}$ as functions of the product $\phi_{c+s}h_{sf}$, which represents the total latent heat storage capacity of the composite. It establishes that the reduction in temperature and temperature gradient afforded by PCM additions depended on this product, rather than ϕ_{c+s} or h_{sf} individually. Note that this would not be the case if the effective thermal conductivity of the pavement was allowed to change with PCM dosage. Also, since the addition of PCMs can negatively impact the mechanical properties (e.g. compressive strength and elastic modulus) of cementitious composites [52,53] – it is beneficial to increase the amount of latent heat storage capacity in the composite by increasing h_{sf} rather than ϕ_{c+s}, as also noted by Šavija and Schlangen [54].

5.3.3. Effect of the concrete's placement temperature

Fig. 8 plots (a) the peak pavement temperature T_{peak} and (b) the peak temperature gradient $T_{x,peak}$ attained within a plain concrete or PCM-composite pavement section as a function of the initial placement temperature T_{init} ranging from 20 °C to 40 °C. Here, the PCM melting temperature varied along with the initial temperature such that the criterion in Eq. (22) was satisfied. As would be expected, the peak temperature decreased linearly with decreasing initial temperature of the concrete. The difference in T_{peak} between the plain concrete and PCM-containing pavements remained similar for each placement temperature considered, indicating that the peak temperature reduction afforded by PCM additions is independent of the concrete's initial temperature. On the other hand, the peak temperature gradient was lowest for an initial temperature $T_{init} = 24$ °C and the difference in $T_{x,peak}$ between plain concrete and PCM-containing sections decreased with decreasing T_{init}.

Taken together, these results suggest that in conjunction with adding PCM, cooling the mixture prior to placement would be the most effective means to mitigate thermal cracking. A simple (and well-known) method of this nature is to add ice to the concrete mixture; whose effectiveness is ensured by the large latent heat associated with melting the ice as well as the large sensible heat capacity of water [3,5]. It should be noted that the optimal choice of the PCM's melting temperature corresponding to $T_{init} = 24$ °C, according to Eq. (22), is $T_{pc} = 28$ °C. Importantly, a PCM with this melting temperature may also inhibit temperature cycling at later ages, where the pavement temperature evolution is largely dictated by the outdoor air temperature. Therefore, the benefit of lowering the initial pavement temperature is twofold: (i) it reduces the maximum temperature and temperature gradient developed within the pavement at early-ages, and (ii) it allows the use of a PCM with a lower melting temperature that could offer benefits associated with reducing thermal fatigue damage.

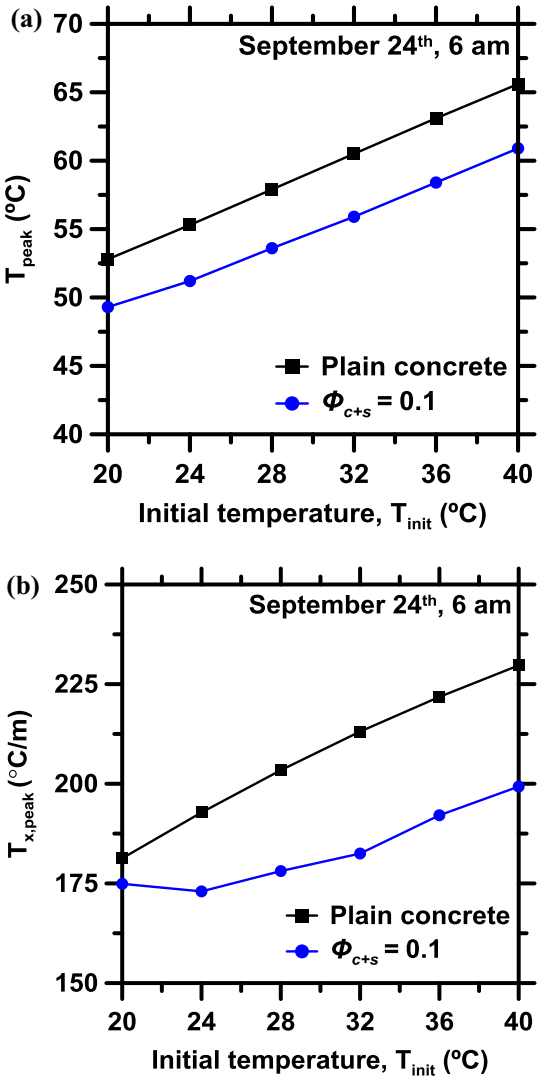

Fig. 8. (a) Peak temperature T_{peak} and (b) peak temperature gradient $T_{x,peak}$ within a plain concrete or PCM-dosed pavement section as a function of the initial temperature T_{init}. Here, the PCM volume fraction was $\phi_{c+s} = 0.1$, the latent heat of fusion was $h_{sf} = 180$ kJ/kg, and the melting temperature window was $\Delta T_{pc} = 8$ °C. The melting temperature T_{pc} was chosen in each case such that $T_{pc} = T_{init} + \Delta T_{pc}/2$.

5.4. Comparison of PCM with high thermal conductivity inclusions

Based on the results presented earlier in Section 5.2, it may be speculated if adding inclusions with a high thermal conductivity (i.e., in an effort to dissipate heat at a higher rate) would be more beneficial to early-age performance than the inclusion of microencapsulated PCM. To investigate this possibility, Fig. 9 plots the maximum temperature $T_{\max}(t)$ within pavement sections made of (i) plain concrete, (ii) concrete with 10 vol.% graphite aggregates, or (iii) concrete with 10 vol.% PCM. Here, the density ρ and specific heat c_p of the graphite used were 2210 kg/m^3 and 709 J/kg K, respectively [39]. The thermal conductivity of the graphite was taken as 20 W/m K [55]. Fig. 9 shows that the peak temperature was reduced only slightly by the inclusion of graphite inclusions, whereas the inclusion of PCM reduced the peak temperature by nearly 5 °C. Therefore, while high thermal conductivity inclusions may increase heat dissipation and/or reduce temperature gradients within the section, they do not show the benefit afforded by the PCM's latent heat storage i.e., in limiting the hydration heat induced temperature rise at early-ages.

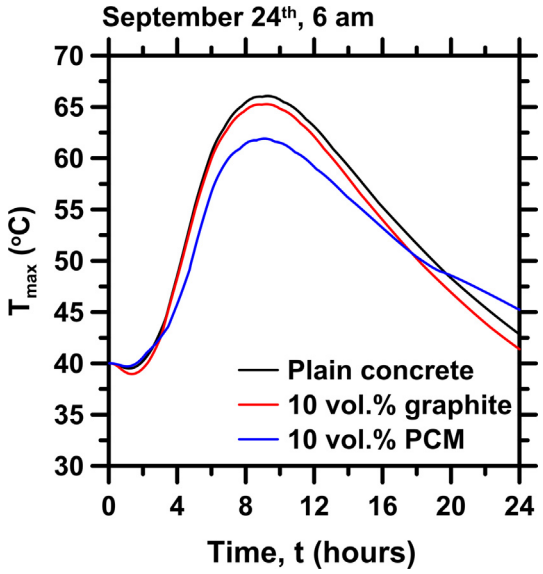

Fig. 9. Maximum temperature $T_{max}(t)$ developed within pavement sections made of plain concrete, concrete with graphite inclusions, or concrete with microencapsulated PCM exposed to outdoor temperature and solar irradiation corresponding to September 24th in Los Angeles, CA and placed at 6 am.

6. Summary and conclusions

This study developed a transient thermal model to predict early-age temperature evolutions within (concrete) pavement sections containing microencapsulated PCMs. Experimental calorimetry data was used to describe the degree of hydration of the cementitious matrix as a function of temperature and time. The degree of hydration data was then used to determine the local rate of heat generation and its influence on pavement temperature evolutions. The inclusion of 10 vol.% microencapsulated PCM within the pavement was shown to induce noticeable reductions in the temperature developed within the first 24 h of placement. Additionally, the addition of PCM also reduced local temperature gradients developed within the pavement section so long as the effective thermal conductivity of the pavement was not reduced. Finally, a parametric study was carried out to assess the effects of different parameters including: melting temperature, latent heat of fusion, and initial pavement temperature, and to suggest a selection criterion for the appropriate choice of PCM melting temperature. These results inform the design and proportioning of PCM-dosed concrete (pavement) mixtures that feature improved resistance to thermal cracking.

Acknowledgements

The authors acknowledge financial support for this work provided by an Infravation ERA-NET Plus Grant (31109806.0001: ECLIPS), National Science Foundation (CMMI:1130028, CAREER: 1253269) and California Energy Commission (Contract: PIR: 12-032). The authors acknowledge financial support provided by The Sustainable L.A. Grand Challenge and the Office of the Vice-Chancellor for Research at UCLA. The contents of this paper reflect the views and opinions of the authors, who are responsible for the accuracy of the datasets presented herein, and not necessarily the views of the funding organizations. The Laboratory for the Chemistry of Construction Materials (LC^2) and the Molecular Instrumentation Center at UCLA acknowledge the support that has made their operations possible.

References

[1] A. Schindler, B.F. McCullough, Importance of concrete temperature control during concrete pavement construction in hot weather conditions, Transp. Res. Rec.: J. Transp. Res. Board 1813 (Jan. 2002) 3–10.
[2] Z. Bofang, Thermal Stresses and Temperature Control of Mass Concrete, Butterworth-Heinemann, 2013.
[3] M.L. Wilson, S.H. Kosmatka, Design and Control of Concrete Mixtures, 15th edition., Portland Cement Assn, Skokie, IL, 2011.
[4] K.L. Lees, K.R. Edwars, Cryogenic Cooling of Concrete, June 8 1971, US Patent 3,583,172.
[5] S. Mindess, J.F. Young, D. Darwin, Concrete, second ed., Pearson, Upper Saddle River, NJ, 2002.
[6] D.P. Bentz, R. Turpin, Potential applications of phase change materials in concrete technology, Cem. Concr. Compos. 29 (7) (2007) 527–532.
[7] F. Fernandes, S. Manari, M. Aguayo, K. Santos, T. Oey, Z. Wei, G. Falzone, N. Neithalath, G. Sant, On the feasibility of using phase change materials (PCMs) to mitigate thermal cracking in cementitious materials, Cem. Concr. Compos. 51 (2014) 14–26.
[8] V.V. Tyagi, D. Buddhi, PCM thermal storage in buildings: a state of art, Renew. Sustain. Energy Rev. 11 (6) (2007) 1146–1166.
[9] L.F. Cabeza, C. Castellon, M. Nogues, M. Medrano, R. Leppers, O. Zubillaga, Use of microencapsulated PCM in concrete walls for energy savings, Energy Build. 39 (2) (2007) 113–119.
[10] M. Solaimanian, T.W. Kennedy, Predicting maximum pavement surface temperature using maximum air temperature and hourly solar radiation, Transp. Res. Rec. 1417 (1993).
[11] A. Hermansson, Simulation model for calculating pavement temperatures including maximum temperature, Transp. Res. Rec.: J. Transp. Res. Board 1699 (2000) 134–141.
[12] C. Yavuzturk, K. Ksaibati, A.D. Chiasson, Assessment of temperature fluctuations in asphalt pavements due to thermal environmental conditions using a two-dimensional, transient finite-difference approach, J. Mater. Civ. Eng. 17 (4) (2005) 465–475.
[13] B.K. Diefenderfer, I.L. Al-Qadi, S.D. Diefenderfer, Model to predict pavement temperature profile: development and validation, J. Transp. Eng. 132 (2) (2006) 162–167.
[14] J. Gui, P.E. Phelan, K.E. Kaloush, J.S. Golden, Impact of pavement thermophysical properties on surface temperatures, J. Mater. Civ. Eng. 19 (8) (2007) 683–690.
[15] C. Ya-ling, S. Yu, W. Zhen-ming, Evaluation on thermal stability of embankments with different strikes in permafrost regions, Cold Reg. Sci. Technol. 58 (3) (2009) 151–157.
[16] Y. Qin, J.E. Hiller, Modeling temperature distribution in rigid pavement slabs: impact of air temperature, Constr. Build. Mater. 25 (9) (2011) 3753–3761.
[17] Y. Qin, J.E. Hiller, Ways of formulating wind speed in heat convection significantly influencing pavement temperature prediction, Heat Mass Transf. 49 (5) (2013) 745–752.
[18] G. De Schutter, Finite element simulation of thermal cracking in massive hardening concrete elements using degree of hydration based material laws, Comput. Struct. 80 (27) (2002) 2035–2042.
[19] R. Faria, M. Azenha, J.A. Figueiras, Modelling of concrete at early ages: application to an externally restrained slab, Cem. Concr. Compos. 28 (6) (2006) 572–585.
[20] M. Azenha, R. Faria, D. Ferreira, Identification of early-age concrete temperatures and strains: monitoring and numerical simulation, Cem. Concr. Compos. 31 (6) (2009) 369–378.
[21] Z. Ge, K. Wang, Z. Gao, Prediction of pavement concrete strength development, joint sawing, and opening time using FEMLAB, J. Perform. Constr. Facil. 26 (2) (2011) 162–169.
[22] ACI, ACI 231R–10 Report on Early-Age Cracking: Causes, Measurement and Mitigation, American Concrete Institute, 2010.
[23] ACI, ACI 207.1R-05 Guide to Mass Concrete, American Concrete Institute, 2005.
[24] P.F. Hansen, J. Pederson, Maturity computer for controlled curing and hardening of concrete strength, Nordisk Betong (1977) 19–34.
[25] ASTM, 11C1702", Standard Test Method for Measurement of Heat of Hydration of Hydraulic Cementitious Materials Using Isothermal Conduction Calorimetry, ASTM International, West Conshohocken, PA, USA, 2015.
[26] G. De Schutter, Applicability of degree of hydration concept and maturity method for thermo-visco-elastic behaviour of early age concrete, Cem. Concr. Compos. 26 (5) (July 2004) 437–443.
[27] A.W. Gutsch, Properties of early age concrete-experiments and modelling, Mater. Struct. 35 (2) (2002) 76–79.
[28] R.C. Tank, N.J. Carino, Rate constant functions for strength development of concrete, Mater. J. 88 (1) (Jan. 1991) 74–83.
[29] Q. Xu, J.M. Ruiz, J. Hu, K. Wang, R.O. Rasmussen, Modeling hydration properties and temperature developments of early-age concrete pavement using calorimetry tests, Thermochim. Acta 512 (1) (2011) 76–85.
[30] A.M. Thiele, A. Kumar, G. Sant, L. Pilon, Effective thermal conductivity of three-component composites containing spherical capsules, Int. J. Heat Mass Transf. 73 (2014) 177–185.
[31] A.M. Thiele, G. Sant, L. Pilon, Diurnal thermal analysis of microencapsulated PCM-concrete composite walls, Energy Convers. Manage. 93 (2015) 215–227.

[32] J.D. Felske, Effective thermal conductivity of composite spheres in a continuous medium with contact resistance, Int. J. Heat Mass Transf. 47 (14) (2004) 3453–3461.
[33] S.N. Al-Saadi, Z.J. Zhai, Modeling phase change materials embedded in building enclosure: a review, Renew. Sustain. Energy Rev. 21 (2013) 659–673.
[34] A.M. Thiele, Z. Wei, G. Falzone, B.A. Young, N. Neithalath, G. Sant, L. Pilon, Figure of merit for the thermal performance of cementitious composites containing phase change materials, Cem. Concr. Compos. 65 (2016) 214–226.
[35] ASTM, "C150", Standard Specification for Portland Cement, ASTM International, West Conshohocken, PA, USA, 2016.
[36] ASTM, "C305", Standard Practice for Mechanical Mixing of Hydraulic Cement Pastes and Mortars of Plastic Consistency, ASTM International, West Conshohocken, PA, USA, 2014.
[37] MPCM Technical Information, Tech. Rep., Microtek Laboratories Inc., Dayton, OH.
[38] Materials in Use in U.S. Highways, Tech. Rep., United States Geological Survey, 2006.
[39] T.L. Bergman, A.S. Lavine, F.P. Incropera, D.P. DeWitt, Fundamentals of Heat and Mass Transfer, seventh ed., John Wiley & Sons, New York City, NY, 2011.
[40] P.W. O'Callaghan, S.D. Probert, Sol-air temperature, Appl. Energy 3 (4) (Oct. 1977) 307–311.
[41] X. Pang, D.P. Bentz, C. Meyer, G.P. Funkhouser, R. Darbe, A comparison study of Portland cement hydration kinetics as measured by chemical shrinkage and isothermal calorimetry, Cem. Concr. Compos. 39 (2013) 23–32.
[42] H.F.W. Taylor, Cement Chemistry, second ed., Thomas Telford Publishing, 1997.
[43] PureTemp 20 Technical Information, Tech. Rep., Entropy Solutions Inc., Minneapolis, MN, 2011. <www.puretemp.com>.
[44] Mitigation Strategies for Design Exceptions – Safety, Tech. Rep., Federal Highway Administration, 2014.
[45] UCLA Energy Design Tools Group, Climate Consultant, 2014. <http://www.energy-design-tools.aud.ucla.edu>.
[46] R.K. Wolfe, G.L. Heath, D.C. Colony, Cooling curve prediction of asphaltic concrete, J. Transp. Eng. 109 (1) (1983) 137–147.
[47] T. Oey, A. Kumar, J.W. Bullard, N. Neithalath, G. Sant, The filler effect: the influence of filler content and surface area on cementitious reaction rates, J. Am. Ceram. Soc. 96 (6) (2013) 1978–1990.
[48] H. Zhang, X. Wang, D. Wu, Silica encapsulation of n-octadecane via sol-gel process: a novel microencapsulated phase-change material with enhanced thermal conductivity and performance, J. Colloid Interface Sci. 343 (1) (2010) 246–255.
[49] S. Yu, X. Wang, D. Wu, Microencapsulation of n-octadecane phase change material with calcium carbonate shell for enhancement of thermal conductivity and serving durability: synthesis, microstructure, and performance evaluation, Appl. Energy 114 (2014) 632–643.
[50] M. Aguayo, S. Das, C. Castro, N. Kabay, G. Sant, N. Neithalath, Porous inclusions as hosts for phase change materials in cementitious composites: characterization, thermal performance, and analytical models, Constr. Build. Mater. 134 (2017) 574–584.
[51] B. Young, A.M. Thiele, A. Fujii, G. Sant, L. Pilon, Thermophysical Properties of Phase Change Materials, 2013. <www.seas.ucla.edu/pilon/downloads.htm>.
[52] B.A. Young, A.M.K. Fujii, A.M. Thiele, A. Kumar, G. Sant, E. Taciroglu, L. Pilon, Effective elastic moduli of core-shell-matrix composites, Mech. Mater. 92 (2016) 94–106.
[53] G. Falzone, G.P. Falla, Z. Wei, M. Zhao, A. Kumar, M. Bauchy, N. Neithalath, L. Pilon, G. Sant, The influences of soft and stiff inclusions on the mechanical properties of cementitious composites, Cem. Concr. Compos. 71 (2016) 153–165.
[54] B. Šavija, E. Schlangen, Use of phase change materials (PCMs) to mitigate early age thermal cracking in concrete: theoretical considerations, Constr. Build. Mater. 126 (2016) 332–344.
[55] L. Lu, B. Ping, Y. He, Q. Ding, F. Wang, H. Zhu, Preparation and properties of alkali-activated ground-granulated blast furnace slag thermal storage concrete, in: International Conference on Durability of Concrete Structures, July 2014.
[56] R.K. Rajput, Engineering Materials & Metallurgy, first ed., S. Chand Limited, New Delhi, India, 2006.
[57] N. Ukrainczyk, S. Kurajica, J. Sipusic, Thermophysical comparison of five commercial paraffin waxes as latent heat storage materials, Chem. Biochem. Eng. Q. 24 (2) (2010) 129–137.